Role of the [Fe_4S_4] Cluster in Mediating Disulfide Reduction in Spinach Ferredoxin:Thioredoxin Reductase†

Christopher R. Staples,‡ Eric Gaymard,§ Anne-Lise Stritt-Etter,§ Joshua Telser,|| Brian M. Hoffman,⊥ Peter Schürmann,§ David B. Knaff,# and Michael K. Johnson*,‡

Department of Chemistry and the Center for Metalloenzyme Studies, University of Georgia, Athens, Georgia 30602, Laboratoire de Biochimie Végétale, Université de Neuchâtel, CH-2007 Neuchâtel, Switzerland, Chemistry Program, Roosevelt University, Chicago, Illinois 60605, Department of Chemistry, Northwestern University, Evanston, Illinois 60208, and Department of Chemistry and Biochemistry, Texas Tech University, Lubbock, Texas 79409

Received December 3, 1997

ABSTRACT: Thioredoxin reduction in plant chloroplasts is catalyzed by a unique class of disulfide reductases which use a one-electron donor, $[Fe_2S_2]^{2+,+}$ ferredoxin, and has an active site involving a disulfide in close proximity to a $[Fe_4S_4]^{2+}$ cluster. In this study, spinach ferredoxin:thioredoxin reductase (FTR) reduced with stoichiometric amounts of reduced benzyl viologen or frozen under turnover conditions in the presence of thioredoxin is shown to exhibit a slowly relaxing $S = 1/2$ resonance ($g = 2.11, 2.00, 1.98$) identical to that of a modified form of the enzyme in which one of the cysteines of the active-site disulfide is alkylated with *N*−ethylmaleimide (NEM−FTR). Hence, in accord with the previous proposal [Staples, C.R., Ameyibor, E., Fu, W., Gardet-Salvi, L., Stritt-Etter, A.-L., Schürmann, P., Knaff, D.B., and Johnson, M.K. (1996) *Biochemistry 35*, 11425−11434], NEM−FTR is shown to be a stable analogue of a one-electron-reduced enzymatic intermediate. The properties of the Fe-S cluster in NEM−FTR have been further investigated by resonance Raman and electron nuclear double resonance spectroscopies; the results, taken together with the previous UV−visible absorption, variable temperature magnetic circular dichroism, and resonance Raman data, indicate the presence of a novel type of $[Fe_4S_4]^{3+}$ cluster that is coordinated by five cysteinates with little unpaired spin density delocalized onto the cluster-associated cysteine of the active-site disulfide. While the ligation site of the fifth cysteine remains undefined, the best candidate is a cluster bridging sulfide. On the basis of the spectroscopic and redox results, mechanistic schemes are proposed for the benzyl viologen-mediated two-electron-reduction of FTR and the catalytic mechanism of FTR. The catalytic mechanism involves novel S-based cluster chemistry to facilitate electron transfer to the active-site disulfide resulting in covalent attachment of the electron-transfer cysteine and generation of the free interchange cysteine that is required for the thiol−disulfide interchange reaction with thioredoxin.

Chloroplast ferredoxin:thioredoxin reductase (FTR)[1] catalyzes a key step in light regulation of several carbon assimilation enzymes in oxygenic photosynthesis (*1, 2*). Electrons are transmitted from the light-harvesting thylakoid membranes to a 2Fe ferredoxin (Fd) and then utilized to cleave the disulfide in thioredoxin *f*, which in turn activates or deactivates a number of target enzymes by reduction of regulatory disulfide bridges (*3*). FTR catalyzes the two-electron-reduction of the active-site disulfide of thioredoxin *f* in sequential one-electron steps with the 2Fe Fd as the one-electron-donor. The enzyme (previously known as ferralterin) is an $\alpha\beta$ heterodimer. The variable or α subunit (7−13 kDa) differs in size (*4, 5*) and shows little or no immunological cross reactivity among different species (*6, 7*). In contrast, the catalytic or β subunit (13 kDa) is highly conserved among different species (*5, 8, 9*) and contains the active-site disulfide in close proximity to a [Fe_4S_4] cluster (*6, 8, 10*).

The role and accessibility of the seven conserved cysteine residues in the catalytic subunit has been addressed by extensive studies of spinach FTR with radiolabeled cysteine alkylating agents (*8*), and the picture of the active site that emerges from these studies is summarized in Figure 1. The active-site disulfide (Cys54-S-S-Cys84) is clearly in close proximity to the [Fe_4S_4] cluster, since a single residue

† This work was supported by grants from the National Institutes of Health (GM51962 to M.K.J. and HL13531 to B.M.H.), the National Science Foundation (DMB-8907559 to B.M.H.), the Schweizerischer Nationalfonds (31-47107.96 and 31-37725.93 to P.S.), the U.S. Department of Energy (DE-FG03-93ER20125 to D.B.K.), and a NSF Research Training Group Award to the Center for Metalloenzyme Studies (BIR9413236 to M.K.J.).

* Author to whom correspondence should be addressed. Telephone: (706) 542-9378. Fax: (706) 542-2353. E-mail: johnson@sunchem.chem.uga.edu.

‡ University of Georgia.

§ Université de Neuchâtel.

|| Roosevelt University.

⊥ Northwestern University.

Texas Tech University.

[1] Abbreviations: FTR, ferredoxin:thioredoxin reductase; T, thioredoxin; NEM, *N*-ethylmaleimide; NEM−FTR, a modified form of FTR with NEM covalently attached at one of the cysteines of the active-site disulfide; (VT)MCD, (variable-temperature) magnetic circular dichroism; RR, resonance Raman; ENDOR, electron nuclear double resonance; Fd, ferredoxin; NHE, normal hydrogen electrode; CW, continuous wave; DTT, dithiothreitol; HiPIP, high potential iron-sulfur protein.

S0006-2960(97)02976-0 CCC: $15.00
Published on Web 03/17/1998

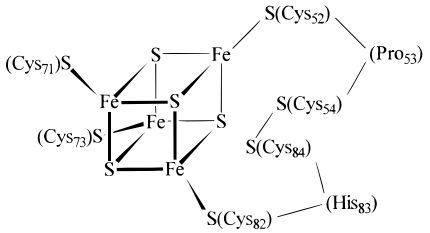

FIGURE 1: Schematic depiction of the active site of FTR as deduced from cysteine alkylation experiments (*8*) and spectroscopic studies (*10*).

separates each of the disulfide cysteines from a cluster-coordinating cysteine. In common with the majority of flavoprotein disulfide reductases (*11*), only one of the cysteines of the active-site disulfide (Cys54) is readily accessible to alkylating reagents such as *N*-ethylmaleimide (NEM). In the case of flavoprotein disulfide reductases, the other active-site cysteine is protected from alkylation by covalent attachment to the flavin isoalloxazine ring (*11*). The present study indicates that the [Fe_4S_4] cluster similarly protects Cys84 from alkylation in NEM-modified FTR (NEM−FTR). Moreover, the mechanism by which Cys84 is protected from alkylation is shown to lie at the heart of understanding the role of the cluster in mediating disulfide reduction in native FTR via two one-electron steps.

The nature and properties of the Fe-S center in spinach FTR and NEM−FTR have been recently been established by UV−visible absorption, variable temperature magnetic circular dichroism (VTMCD), EPR, and resonance Raman (RR) spectroscopies (*10*). These studies revealed the presence of a single diamagnetic ($S = 0$) [Fe_4S_4]$^{2+}$ cluster in native FTR. The [Fe_4S_4]$^{2+}$ cluster can be partially oxidized to the $S = 1/2$ [Fe_4S_4]$^{3+}$ state by potassium ferricyanide (0.3 spin/molecule), but this [Fe_4S_4]$^{3+,2+}$ redox process is unlikely to be physiologically relevant, since the midpoint potential ($E_m \sim +420$ mV versus NHE) is > 600mV higher than that of either the natural electron donor, spinach Fd ($E_{m(n=1)} = -420$ mV), or the active-site disulfide ($E_{m(n=2)} = -230$ mV) (*12*). Furthermore, the cluster is not reducible to the paramagnetic [Fe_4S_4]$^{+}$ state using excess dithionite, reduced benzyl or methyl viologen, dithiothreitol (DTT), or deazaflavin-mediated photoreduction, indicating a potential < −650 mV versus NHE (*10*). Hence a purely electron transfer role for the cluster is considered to be extremely unlikely (*6*, *10*). However, reduced benzyl or methyl viologen, although not dithionite alone, was shown to function as a nonphysiological electron donor, effecting the two-electron-reduction of the active-site disulfide in FTR (*13*). The conundrum that therefore needs to be rationalized by any mechanistic scheme is how this reduction can occur in two one-electron steps without involving a reduced, [Fe_4S_4]$^{+}$, cluster.

The first major insight into the role of the [Fe_4S_4] cluster in FTR came from the markedly different spectroscopic properties of NEM−FTR compared to those of native FTR (*10*). As-prepared NEM−FTR exhibits an EPR signal with unusual properties; it has anomalous *g*-value anisotropy ($g = 2.112, 1.997, 1.984$) and is observable without broadening at temperatures up to at least 150 K. Based on RR and VTMCD data (*10*), the EPR signal was assigned to an oxidized, $S = 1/2$ [Fe_4S_4]$^{3+}$ cluster, albeit with quite different properties from an $S = 1/2$ [Fe_4S_4]$^{3+}$ cluster in high potential iron-sulfur proteins (HiPIPs) (typically, $g = 2.12, 2.04, 2.02$ and observable only at temperatures < 30 K (*14*−*16*). Furthermore, this [Fe_4S_4]$^{3+}$ cluster was reducible to the $S = 0$ [Fe_4S_4]$^{2+}$ state with a midpoint potential of −210 mV versus NHE, 630 mV lower than the corresponding potential for the native cluster (and ∼ +250 to +650 mV lower than in HiPIPs (*14*−*16*). The cluster's remarkably low midpoint potential and uncharacteristic EPR properties were attributed to the association of the active-site cysteinyl residue, Cys84, that is protected from alkylation, while Cys54 is alkylated and noninteracting. Since a [Fe_4S_4]$^{3+}$ cluster with a covalently attached fifth cysteinato ligand is isoelectronic with a [Fe_4S_4]$^{2+}$ cluster and a nearby cysteinyl radical, we envisaged NEM−FTR as a resonance hybrid of these two canonical forms (*10*). One-electron-reduction of NEM−FTR then results in a diamagnetic [Fe_4S_4]$^{2+}$ cluster and a free cysteinate, (Cys84)S^-, in accord with the experimental observations.

This model for NEM−FTR can be directly applied to native FTR. The resting-state enzyme contains the [Fe_4S_4]$^{2+}$ cluster with a nearby disulfide [(Cys84)S-S(Cys54)]. One-electron-reduction yields an intermediate that can analogously be represented as a diamagnetic [Fe_4S_4]$^{2+}$ cluster with a stabilized cysteinyl radical, (Cys84)$S^{\bullet}$ (plus a free cysteinate, (Cys54)S^-), with the alternate limiting resonance form being a paramagnetic [Fe_4S_4]$^{3+}$ cluster with an associated cysteinate, (Cys84)S^- (plus a free cysteinate, (Cys54)S^-). The second electron then effects complete reduction of the active-site disulfide. Thus NEM−FTR might be an analogue of the one-electron-reduced enzymatic intermediate in which the cluster formally stabilizes the cysteinyl radical, (Cys84)-$S^{\bullet}$,while creating a cysteinate, (Cys54)S^-, that is free to attack and form a heterodisulfide intermediate with the substrate. One prediction of this hypothesis is that one-electron-reduction of native FTR will lead to net one-electron-oxidation of the resting-state [Fe_4S_4]$^{2+}$ cluster and a species similar to that found in as-prepared NEM−FTR.

To test this hypothesis and investigate further the role of the cluster in FTR, we have undertaken preliminary freeze-quench EPR studies of FTR under turnover conditions and EPR studies of FTR reduced with stoichiometric amounts of reduced benzyl viologen. These experiments indicate that NEM−FTR is indeed a stable analogue of the one-electron-reduced enzymatic intermediate. In addition, we have used electron nuclear double resonance (ENDOR) spectroscopy to investigate which of the two proposed canonical forms represents the best description of NEM−FTR and extended the range of our RR studies in an attempt to assess the possibility of a novel μ_3-S−S(Cys) mode of attachment for the protected cysteine. The mechanism of active-site disulfide reduction by benzyl viologen and the catalytic mechanism of thioredoxin reduction are discussed in light of these new results. All the available evidence points to a direct role for the [Fe_4S_4] cluster in FTR in cleaving the active-site disulfide, and we conclude that this new role most likely involves S-based cluster chemistry.

MATERIALS AND METHODS

Sample Preparation and Handling. The purification and assay procedures used in preparing samples of spinach (*Spinacea oleracea*) native and recombinant FTR and thiore-

doxin *f* have been described in detail elsewhere (*17, 18*). The properties and spectroscopic characteristics of the recombinant FTR were indistinguishable from those of the native protein. NEM modification of one of the cysteines of the active-site disulfide of FTR was carried out as previously described (*8, 19*). The samples of NEM-modified FTR used in this work had A_{410}/A_{280} ratios in the range 0.34−0.36 and were >90% pure as judged by SDS−PAGE gel electrophoresis. Sample concentrations for native FTR and NEM−FTR are based upon $\epsilon_{410} = 17\,400\ M^{-1}\ cm^{-1}$ (*6*) and $\epsilon_{410} = 19\,500\ M^{-1}\ cm^{-1}$ (*19*), respectively. Unless otherwise stated, native FTR was in 20 mM phosphate buffer, pH 7.2; NEM−FTR was in 20 mM triethanolamine hydrochloride buffer, pH 7.3; all samples were handled anaerobically in a Vacuum Atmospheres glovebox or a gas handling line under an Ar atmosphere (<1 ppm O_2). Benzyl viologen-mediated reduction and turnover of FTR were carried out under anaerobic conditions using a freshly prepared stock solution of dithionite-reduced benzyl viologen in 30:70 ethanol/water (v/v). The concentration of the stock solution was determined spectrophotometrically. The ENDOR samples of *Chromatium vinosum* and *Ectothiorhodospira halophila* HiPIPs were kindly provided by Dr. M. C. Kennedy (Medical College of Wisconsin) and Drs. T. E. Meyer and M. A. Cusanovich (University of Arizona), respectively.

Spectroscopic Measurements. X-band (~9.6 GHz) EPR spectra were recorded on a Bruker ESP300E spectrometer equipped with an ER-4116 dual mode cavity and an Oxford Instruments ESR-9 flow cryostat. EPR quantitations were carried out under nonsaturating conditions using 1 mM CuEDTA as the standard. Raman spectra were recorded with an Instruments SA U1000 spectrometer fitted with a cooled RCA 31034 photomultiplier tube, using lines from Coherent Innova 10-W Ar^+ or Kr^+ lasers. Scattering was collected at 90° from the surface of a frozen 10 μL droplet of protein in a specially constructed anaerobic cell (*20*) mounted on the coldfinger of an Air Products Displex model CSA-202E closed cycle refrigerator. Band positions were calibrated using the excitation wavelength and a Na_2SO_4 reference solution and are accurate to $\pm 1\ cm^{-1}$.

Continuous wave (CW) "Q"-band (35 GHz) EPR/ENDOR spectra were recorded on a modified Varian E-109 spectrometer at 2 K in the dispersion mode using 100 kHz field modulation as described elsewhere (*21*). Under these "rapid-passage" conditions, the EPR spectra represent the actual absorption envelope, rather than its derivative. ENDOR signals were enhanced by application of rf broadening as described previously (*22*). Pulsed Q-band spectra were recorded on a locally built spectrometer that has been previously described (*23*). The Mims pulse sequence was generally employed (*24*).

The single-crystal ENDOR transition frequencies for a nucleus, *J*, of spin $I = 1/2$, with low g_N such as ^{57}Fe are given to first order by eq 1 (*25*):

$$\nu_{\pm} = |A^J/2 \pm \nu_J| \qquad (1)$$

where A^J is the orientation-dependent nuclear hyperfine coupling constant and ν_J is the nuclear Larmor frequency. For $\nu_J > A^J/2$, as is generally the case for ^1H, then the ENDOR spectrum consists of a hyperfine-split doublet centered at the Larmor (NMR) frequency. Nuclei with $I >$ 1/2, such as ^2H and ^{14}N (both $I = 1$), also exhibit quadrupole coupling, which to first order, gives $2I$ lines for each hyperfine or Larmor-split doublet (*25*). Computer simulation and analysis of frozen-solution ENDOR spectra employed procedures and programs described elsewhere (*26, 27*).

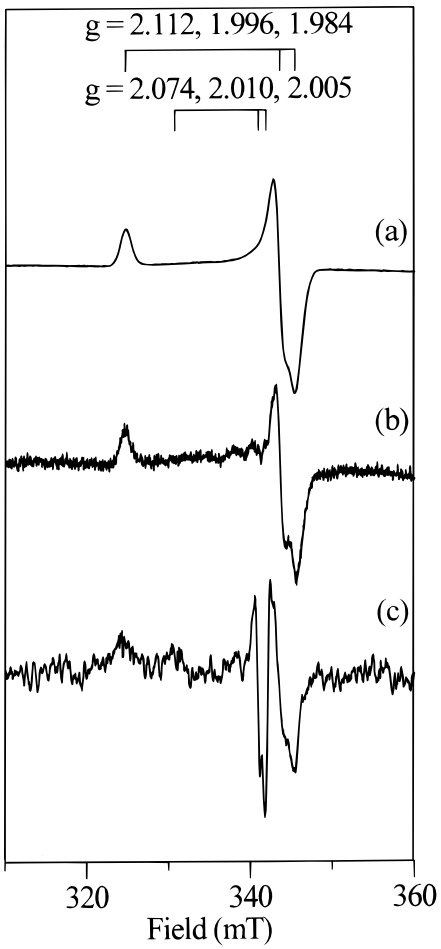

FIGURE 2: X-band EPR spectra of spinach FTR. (a) NEM−FTR as prepared (120 μM). (b) Native FTR (442 μM) reduced with 1 equiv of reduced benzyl viologen. (c) Native FTR frozen during enzyme turnover (see text for details). EPR conditions: temperature, 35 K; microwave power, 1 mW; modulation amplitude, 0.63 mT; microwave frequency, 9.60 GHz.

RESULTS

EPR Studies of Native FTR. Dithionite alone is unable to effect reduction of the active-site disulfide in FTR, and all attempts to elicit an EPR signal by reducing native FTR using dithionite proved unsuccessful. These experiments included using sub-stoichiometric, stoichiometric, and excess (up to 100-fold) dithionite at pH values in the range 7−10. However, addition of a stoichiometric amount of reduced benzyl viologen to native FTR produces an EPR signal indistinguishable from that of NEM−FTR, i.e., $g = 2.112$, 1.996, 1.984 and observable up to ~150 K (Figure 2b). This resonance maximally accounts for 0.1 spin/molecule and is not observed in samples reduced with > 2 equiv of reduced benzyl viologen. Since excess reduced benzyl viologen is known to effect reduction of the active-site disulfide (*13*), this similarity in EPR signals supports the view that NEM−FTR is a stable analogue of a one-electron-reduced form of FTR.

To assess if the one-electron-reduced form of FTR also is present during catalytic turnover, preliminary freeze-quench EPR experiments were conducted in the presence of substrate. These experiments involved mixing FTR, thioredoxin *f*, and dithionite in the mole ratio 1:4:12 in an anaerobic 50 mM Tris·HCl buffer, pH 7.8, to give a final FTR concentration of 75 μM and initiating the reaction by addition of benzyl viologen (final concentration of 20 μM). Samples frozen prior to the addition of benzyl viologen exhibited no EPR signals, and samples frozen more than 1 min after the addition of benzyl viologen only showed a weak benzyl viologen radical signal centered at $g = 2.004$. However, samples frozen within 5 s of the addition of benzyl viologen, exhibited two weak $S = 1/2$ resonances that together account for <0.05 spin/molecule (Figure 2c). The major signal is readily identified by its g values, $g = 2.11, 2.00, 1.98$, as the one-electron-reduced form of FTR. The minor signal is tentatively identified as an almost axial resonance with $g = 2.07, 2.01, 2.00$. Since neither resonance was observed in control experiments without the substrate, thioredoxin *f*, and both resonances are transient species, we attributed them to intermediates that are present during enzyme turnover. These observations confirm our hypothesis that NEM−FTR corresponds to a stabilized form of a one-electron-reduced FTR reaction intermediate (*10*) and prompted further characterization of the Fe-S cluster in NEM−FTR using RR and ENDOR spectroscopies.

Resonance Raman Studies of Native and NEM-Modified FTR. Resonance Raman spectra of native FTR and NEM−FTR (as-prepared and dithionite-reduced) have been reported with 457.9-nm excitation in the Fe-S stretching region, 240−450 cm^{-1} (*10*). The spectra for FTR and reduced NEM−FTR are very similar and indicative of $[Fe_4S_4]^{2+}$ clusters with complete cysteinyl ligation, while the spectrum of NEM−FTR is characteristic of the one-electron-oxidized $[Fe_4S_4]^{3+}$ cluster (*10*). Since the anomalous properties of NEM−FTR have been attributed to covalent attachment of the protected cysteine (Cys84) of the active-site disulfide (*10*), we have now extended our RR studies of FTR and NEM−FTR to 800 cm^{-1}, in an attempt to find evidence for the S-S stretching mode of a putative μ_3-S-S(Cys) interaction in NEM−FTR. Such a mode might be resonantly enhanced with excitation into S → Fe(III) charge-transfer bands via kinematic coupling with Fe-S stretching modes. Spectra were obtained with 413-, 458-, and 514-nm excitation for both FTR and NEM−FTR, but there are no obvious candidates for a S-S stretching mode in the 480−560 nm region that is unique to NEM−FTR. Weak bands centered at 488 and 554 cm^{-1} are seen in both native FTR and NEM−FTR (Figure 3), and in samples in which the active-site disulfide is fully reduced (data not shown). The only possibility is a weak band at 538 cm^{-1} with 458-nm excitation that is more clearly apparent in NEM−FTR than in native FTR (Figure 3) and is lost on dithionite reduction. However, no reliable assignment can be made without isotope shift data and it has not yet been possible to enrich samples with ^{34}S.

ENDOR Studies of NEM-Modified FTR. The well-defined rhombic g-tensor for NEM−FTR permits examination of the orientation dependence of the ^1H ENDOR signals for this system. Figure 4 shows ^1H ENDOR spectra of NEM−FTR taken at each of the canonical g-values, $g_{1,2,3} = 2.11, 1.99, 1.98$, and the Q-band EPR spectrum is shown as an inset. The spectra were recorded using conditions to maximize strongly coupled ^1H signals, with a resulting slight loss of resolution. The ^1H-ENDOR pattern consists of poorly resolved features from numerous ^1H nuclei with maximum coupling $A(^1H) \lesssim 15$ MHz.

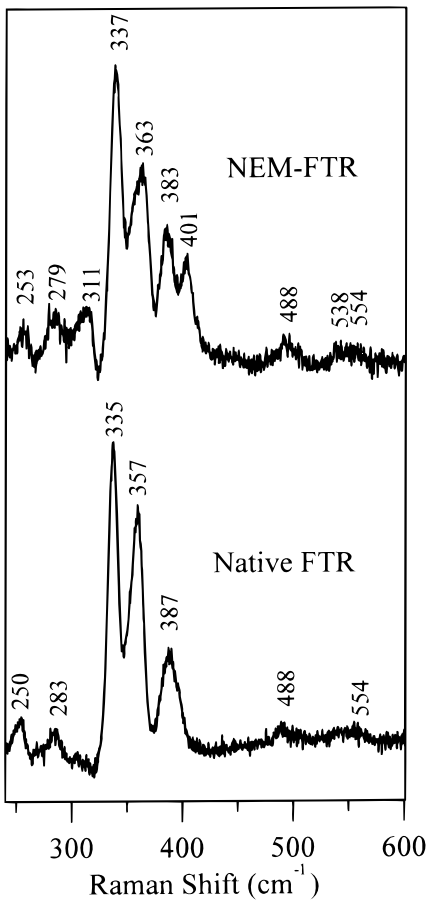

FIGURE 3: Resonance Raman spectra of native and NEM-modified FTR. Both spectra were recorded for samples (~ 2 mM) frozen at ~30 K using 457.9-nm laser excitation with 70 mW laser power at the sample. Each scan involved photon counting for 1 s at 0.4 cm^{-1} increments with 0.6 cm^{-1} spectral resolution, and the spectra shown correspond to the sum of 70 scans. For both spectra, vibrational modes originating from the frozen buffer solution have been subtracted after normalizing the intensities of the "ice-band" at 231 cm^{-1}, and a linear ramp fluorescence background has been subtracted.

Comparison of the CW ^1H ENDOR spectra of NEM−FTR in H_2O buffer with those for protein in D_2O buffer using the same experimental conditions (data not shown) indicates that none of the couplings with $A(^1H) > 2$ MHz is solvent-exchangeable. CW ^2H ENDOR spectra of the D_2O samples exhibit the characteristic signal centered at the deuteron Larmor frequency, $\nu(^2H) = 8.2$ MHz at g_2, arising from unresolved, weakly coupled ^2H in the cluster vicinity, as in other Fe-S proteins, including *C. vinosum* HiPIP (*28*). Pulsed (Mims) ENDOR spectra show weakly coupled ^2H signals (Figure 5A shows the signal at g_2), with maximum signal breadth ~0.7 MHz, which yields a maximum hyperfine coupling for solvent-exchangeable hydrogens, $A(^1H_{exch}) \approx 3.5$ MHz.[2] A similar signal observed for the $[Fe_3S_4]^+$ cluster in *Desulfovibrio gigas* hydrogenase was attributed to amide N-H···S hydrogen bonds (*29*). Comparable ^2H Mims ENDOR signals have also been seen for aconitase (*30*) and

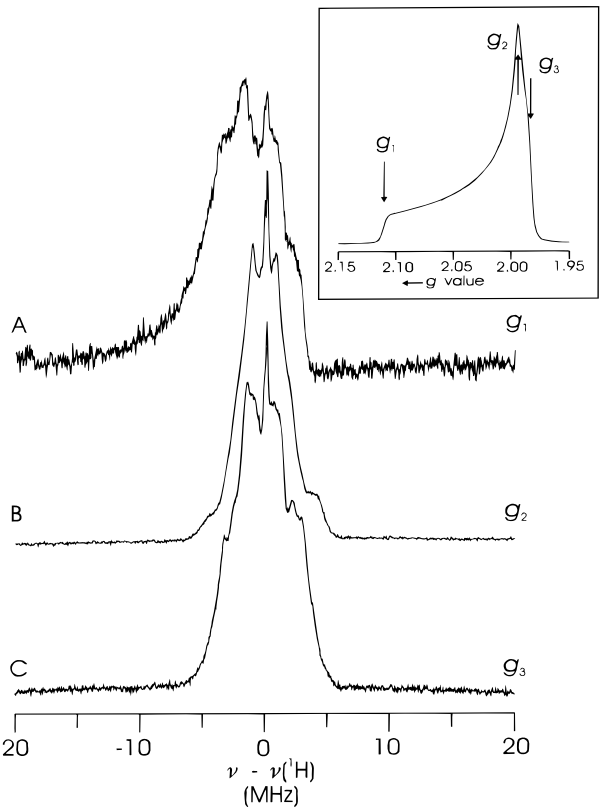

FIGURE 4: Q-band CW ^{1}H ENDOR spectra of NEM-modified FTR (220 μM) at each of the three canonical g values. Experimental conditions: (A) temperature, 2 K; microwave frequency, 35.023 GHz; microwave power, 6.3 μW; magnetic field, 1.1850 T (g = 2.112; g_1); 100 kHz field modulation amplitude, 0.21 mT; time constant, 64 ms; rf scan rate, −0.5 MHz/s; rf power, 20 W; number of scans, 50. (B) as in (A) except: magnetic field, 1.2540 T (g = 1.995; g_2). (C) as in (A) except: magnetic field, 1.2610 T (g = 1.984; g_3). Inset: Q-band CW EPR spectrum used for obtaining the ENDOR spectra. The spectrum was recorded under rapid-passage conditions and thus has an absorption line shape.

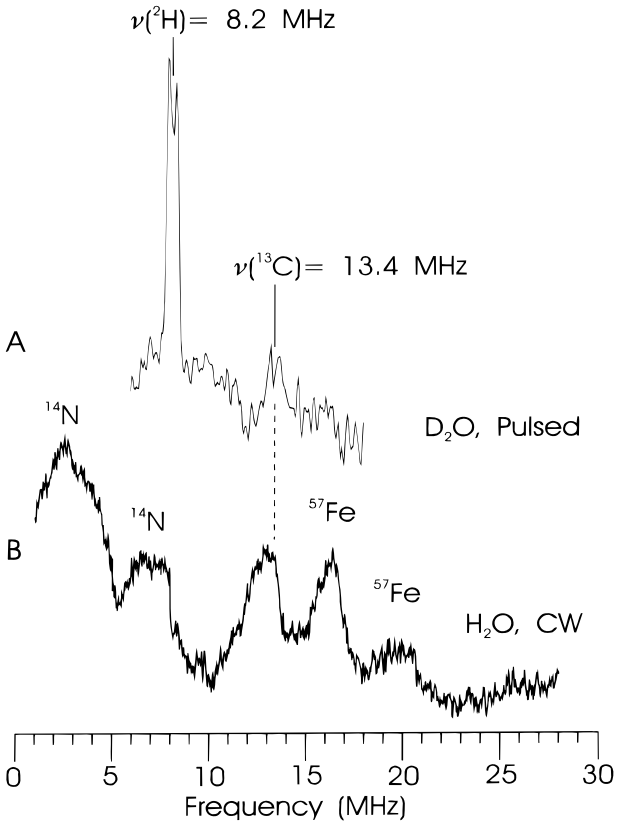

FIGURE 5: Q-Band ENDOR taken at g_2 of the low-frequency region of NEM−FTR (∼ 200 μM) prepared in D_2O-exchanged buffer using pulsed (Mims) ENDOR (A), and in H_2O buffer using CW ENDOR (B). The signals are identified by nucleus according to their likely source (see text) and the Larmor frequencies of ^{2}H and ^{13}C are indicated. Experimental conditions: (A) temperature, 2 K; microwave frequency, 34.884 GHz; magnetic field, 1.2510 T (g = 1.992; g_2); Mims sequence, $\pi/2$ microwave pulse widths (t_p), 80 ns; τ_{12}, 380 ns; rf pulse width (t_{rf}), 50 μs; rf power, 200 W (3−8 dB); repetition rate, 20 Hz; 200 transients; (B) temperature, 2 K; microwave frequency, 35.023 GHz; microwave power, 6.3 μW (45 dBm); magnetic field, 1.2540 T (g = 1.995; g_2); 100 kHz field modulation amplitude, 0.21 mT; time constant, 32 ms; rf scan rate, −0.5 MHz/s; rf power, 20 W; number of scans, 50.

Pyrococcus furiosus 3Fe and 4Fe Fds (J. Telser, H. I. Lee, H. Huang, P. Brereton, M. W. W. Adams, and B. M. Hoffman, manuscript in preparation).

The overall appearance of the ^{1}H ENDOR pattern for NEM−FTR is characteristic of that seen for proteins containing $[Fe_4S_4]$ clusters, both in the reduced $[Fe_4S_4]^+$ form (*31, 32*) and in the oxidized $[Fe_4S_4]^{3+}$ form (*28, 32*). This similarity is illustrated in Figure 6, which compares the ^{1}H ENDOR spectra taken at g_2 of NEM−FTR with those of the $[Fe_4S_4]^{3+}$ clusters in the high potential iron proteins (HiPIPs) isolated from *C. vinosum* and *E. halophila* (*28*). Of particular importance is that for all three proteins, the hyperfine couplings that are from β-^{1}H nuclei on the cysteinyl ligands (*27*−*29, 33*), fall within the range $0 < A(^1H) < \sim 12-14$ MHz. Likewise, in the $[Fe_4S_4]^{3+}$ species prepared by γ-irradiation of the diamagnetic model compound, $[(C_2D_5)_4N]_2[Fe_4S_4(SCH_2C_6D_5)_4]$, the complete $A(^1H)$ tensors for all eight thiolate hydrogens have been determined, and all components have $A_i(^1H) < 11$ MHz (*33*). In contrast, EPR studies of cysteinyl radicals, (Cys)S$^\bullet$, generated by γ-irradiation of a single-crystal of L-cystine dihydrochloride, show that the β-^{1}H nuclei exhibit significantly larger couplings, with the largest component of $A(^1H) \approx 50-60$ MHz (*34*).

Despite low isotopic abundance in unenriched samples, ENDOR signals from both natural-abundance ^{13}C and ^{57}Fe are generally observable in Fe-S proteins, as confirmed by isotopic enrichment (*28*). Also observable in many Fe-S proteins are ENDOR signals from noncoordinated, but magnetically coupled, ^{14}N of polypeptide backbone amide nitrogens that are involved in hydrogen-bonding to the cluster (*28*). Figure 5 presents ENDOR spectra for NEM−FTR over the radio frequency region that encompasses these signals. The CW ENDOR spectrum of NEM−FTR in H_2O buffer, Figure 5B, shows a ^{13}C signal at $\nu(^{13}C) \approx 13$ MHz, analogous to previous results for Fe-S proteins (*28*). This assignment is confirmed using Q-band pulsed Mims ENDOR, which suppresses more strongly coupled resonances (*29, 35*), so that only weakly coupled signals due to ^{2}H (see above) and natural abundance ^{13}C are readily seen in this radio-frequency region, (Figure 5A).

In the CW spectrum, Figure 5B, there are peaks at ∼16 and ∼19 MHz that are from strongly coupled, natural-

[2] This value is calculated by taking the maximum signal breadth for ^{2}H (0.72 MHz) and subtracting the effect of quadrupole coupling (*25*−*27*) typical for hydrogen-bonded ^{2}H, $3P \approx 0.18$ MHz (*29*), and converting this value to ^{1}H coupling: $A(^1H_{exch}) = A(^2H)(g_H/g_D) = (0.72-0.18)(6.51) = 3.5$ MHz.

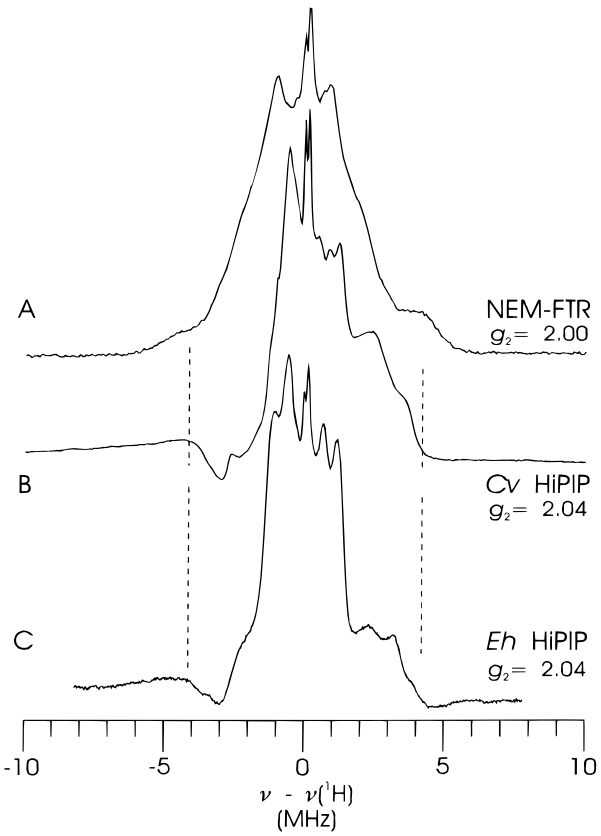

FIGURE 6: Q-band CW ^{1}H ENDOR spectra in H_2O buffer of NEM−FTR (A), *C. vinosum* HiPIP (B), and *E. halophila* HiPIP (C). Experimental conditions: (A) temperature, 2 K; microwave frequency, 35.025 GHz; microwave power, 6.3 μW (45 dBm); magnetic field, 1.2535 T ($g = 1.996$; g_2); 100 kHz field modulation amplitude, 3.3 mT; time constant, 32 ms; rf scan rate, −0.5 MHz/s; rf power, 10 W; number of scans, 20; (B) as in (A) except: microwave frequency, 35.052 GHz; microwave power, 200 μW (30 dBm); magnetic field, 1.2250 T ($g = 2.044$; g_2); 100 kHz field modulation amplitude, 0.7 mT; rf scan rate, −0.5 MHz/s; rf power, 10 W, applied in a 50% duty cycle at 10 kHz; (C) as in (A) except: microwave frequency, 34.924 GHz; microwave power, 20 μW (40 dBm); magnetic field, 1.2260 T ($g = 2.035$; $g_\perp$); 100 kHz field modulation amplitude, 0.11 mT; rf scan rate, −0.4 MHz/s; rf power, 5 W, applied in a 10% duty cycle at 10 kHz. The dashed lines show the maximum breadth of the ^{1}H ENDOR pattern for NEM-modified FTR and corresponding features in the two HiPIPs.

abundance ^{57}Fe. Assignment of each to the ν_+ partner of a Larmor-split ^{57}Fe doublet [$2\nu(^{57}\text{Fe}) \approx 3.5$ MHz, eq 1] gives two Fe sites with $A(^{57}\text{Fe}) \approx 34$ and 28 MHz. Similar signals at ∼16 and ∼20 MHz were reported for both *C. vinosum* and *E. halophila* HiPIPs and were assigned to natural-abundance ^{57}Fe with an average $A(^{57}\text{Fe}) \approx 36$ MHz (*28*). Comparable ^{57}Fe hyperfine couplings have seen by Mössbauer spectroscopy for the $[Fe_4S_4]^{3+}$ cluster in *C. vinosum* HiPIP (*36*) and in ENDOR studies of ^{57}Fe-enriched $[Fe_4S_4]^{3+}$ centers in model complexes (*37*), *C. vinosum* HiPIP (*38*), and *Clostridium pasteurianum* Fd (*39*).

The remaining features in the CW ENDOR spectrum arise from magnetically coupled ^{14}N. The feature at 7−8 MHz is assigned to the $\Delta m_I = \pm 2$ transition of ^{14}N that becomes partially allowed due to state mixing caused by quadrupole coupling. The features at 2−4 MHz are due to the $\Delta m_I = \pm 1$ transition of ^{14}N ($\nu(^{14}\text{N}) = 3.9$ MHz at g_2). Both the $\Delta m_I = \pm 1$ and $\Delta m_I = \pm 2$ transitions include the effects of hyperfine and quadrupole couplings that can in principle be analyzed quantitatively (*40*, *41*). Here we only note their qualitative similarity to previous results. Thus all ENDOR features observed for NEM−FTR can be satisfactorily explained by analogy with conventional Fe-S proteins in general and oxidized HiPIP-type proteins in particular.

DISCUSSION

The results presented above provide major new insights into the role and properties of the [Fe_4S_4] cluster in spinach FTR. First, the observation that FTR reduced with 1 equiv of reduced benzyl viologen produces an EPR signal with line shape, *g*-values, and relaxation properties identical to those of NEM−FTR, confirms our proposal that NEM−FTR corresponds to a stable analogue of a one-electron-reduced form of the native enzyme (*10*). Second, preliminary freeze-quench EPR studies in which the enzyme was frozen under turnover conditions in the presence of thioredoxin *f*, indicate that this one-electron-reduced form of FTR is indeed an intermediate in the catalytic cycle. Third, ENDOR studies show that NEM−FTR is quite similar to proteins and model compounds containing a $[Fe_4S_4]^{3+}$ cluster. This result is in complete accord with UV−visible absorption, VTMCD, and RR characteristics of NEM−FTR (*10*). Hence the anomalous EPR and redox properties of NEM−FTR (i.e., $g = 2.11$, 2.00, 1.98, and observable without broadening at $T \leq 150$ K; $E_{m(3+/2+)} = -210$ mV) compared to $[Fe_4S_4]^{3+}$ clusters in conventional HiPIPs (typically, $g = 2.12$, 2.04, 2.02, observable at $T < 30$ K; $E_{m(3+/2+)}$ in the range +50 to +450 mV (*14*−*16*) and in ferricyanide-oxidized FTR with the active-site disulfide intact ($g = 2.09$, 2.04, 2.01, observable at $T < 30$ K; $E_{m(3+/2+)} \sim +430$ mV (*10*) cannot be rationalized in terms of a $[Fe_4S_4]^{2+}$ cluster with a nearby cysteinyl radical. Rather, the unique properties of the $[Fe_4S_4]^{3+}$ cluster in as-isolated NEM−FTR and one-electron-reduced FTR are attributed to covalent attachment of the protected cysteine (Cys84) of the active-site disulfide.

The paradox that therefore needs to be rationalized by any mechanistic scheme for the disulfide reduction in FTR, is how one-electron *reduction* of FTR leads to one-electron *oxidation* of the $[Fe_4S_4]^{2+}$ cluster. Such anomalous redox behavior is, however, readily explained by invoking two-electron-reduction of the active-site disulfide coupled with one-electron-oxidation of the cluster to yield a species that is formally analogous to NEM−FTR. With this in mind, Figure 7 shows a viable scheme for the benzyl viologen-mediated two-electron-reduction of the active-site disulfide in FTR. The mechanism invokes a role for the cluster both in mediating electron transfer to the active-site disulfide and in stabilizing the one-electron-reduced intermediate via covalent attachment of the electron-transfer cysteine (Cys84) of the active-site disulfide. One-electron-reduction of the cluster leads to transient formation of a $[Fe_4S_4]^{+}$ cluster which immediately cleaves the active-site disulfide via nucleophilic attack involving an electron-rich μ_3-S^{2-}. The resulting cluster is formally at the $[Fe_4S_4]^{3+}$ oxidation level, since two electrons have been withdrawn from the cluster in forming the covalent bond with Cys84 of the active-site disulfide. This one-electron-reduced intermediate is analogous to NEM−FTR, in which alkylation of Cys54 prevents further reactivity. An alternative canonical form of the one-electron intermediate is a $[Fe_4S_4]^{2+}$ cluster with a nearby cysteinyl radical [(Cys84)S•], although the spectroscopic data clearly argue for the unpaired electron density residing on the cluster.

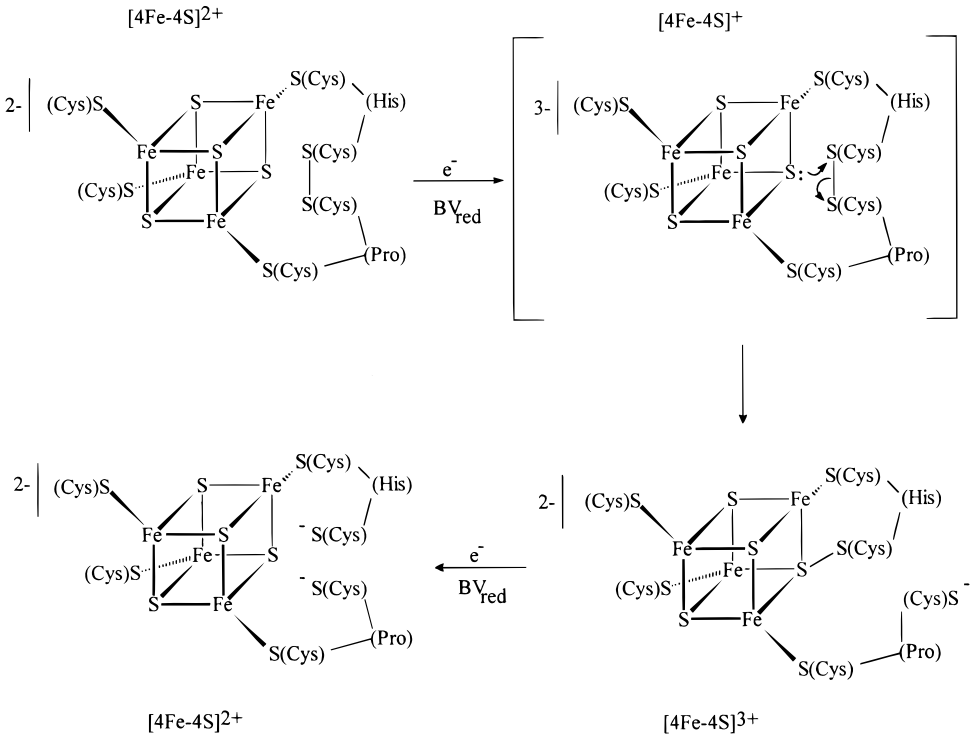

FIGURE 7: Proposed mechanism for the benzyl viologen-mediated two-electron-reduction of FTR.

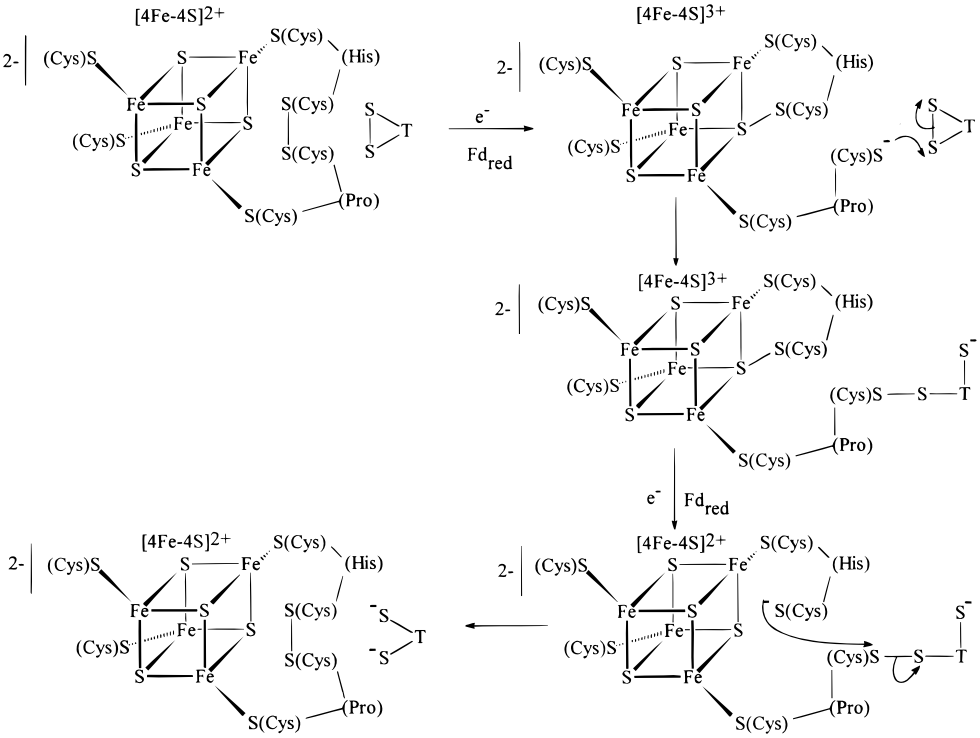

FIGURE 8: Proposed mechanism for FTR, modified from Staples et al. (*10*). Thioredoxin *f* is represented by T.

This intermediate can nevertheless be viewed as a protected cysteinyl radical, wherein the protecting group is the redox-active $[Fe_4S_4]$ cluster. The second reducing equivalent from reduced benzyl viologen then cleaves this μ_3-S-S(Cys84) disulfide to yield the $[Fe_4S_4]^{2+}$ cluster and $(Cys84)S^-$. On the basis of the midpoint potential for the $[Fe_4S_4]^{3+,2+}$ couple in NEM−FTR [−210 mV versus NHE (*10*)], the reduction potential for this second one-electron-reduction is likely to be near the midpoint potential for the two-electron disulfide reduction in FTR [−230 mV versus NHE (*12*)]. The low spin concentration of the intermediate in the native enzyme, maximally 0.1 spin/molecule, suggests that the midpoint potentials for the successive one-electron-reductions for cleavage of the active-site disulfide are within 40 mV of each other.

As yet there is no direct evidence or precedent in Fe-S cluster chemistry for the novel μ_3-S-S(Cys84) disulfide linkage proposed in NEM−FTR. There is a weak band at 538 cm^{-1} in the RR spectrum of NEM−FTR that is a candidate for a cluster-associated S-S stretching mode, since

it is not present in native FTR or dithionite reduced NEM−FTR. However, without ^{34}S-isotope shift data, this assignment must be viewed as speculative at best. An alternative mode of attachment that could lead to a $[Fe_4S_4]^{3+}$ intermediate involves a 5-coordinate Fe site with two coordinated cysteines. Holm and co-workers have synthesized $[Fe_4S_4]$ clusters with bidentate thiolate coordination at a specific Fe site (*42*), and it interesting to note that the midpoint potential for the $[Fe_4S_4]^{3+,2+}$ couple is decreased by 600 mV compared to equivalent monodentate thiolate. The midpoint potential for the $[Fe_4S_4]^{3+,2+}$ couple in NEM−FTR is also ∼600 mV lower than in FTR. While we cannot rule out this alternative mode of cluster attachment for Cys84, there are good reasons for favoring S-based as opposed to Fe-based cluster chemistry. First, it makes chemical sense for the Fe-S cluster to act as the conduit for electron transfer to the disulfide, in which case the bridging sulfides are the only nucleophilic sites on the cluster that can attack and cleave the active-site disulfide with the formation of $[Fe_4S_4]^{3+}$ species. Second, a similar slowly relaxing EPR signal ($g = 2.09, 2.00, 1.98$) has been observed in ferricyanide-oxidized *Azotobacter vinelandii* Fd I and, in this case, the crystal structure of the native Fd indicates that the S_γ of a free cysteine is located 3.4 Å from a μ_3-S^{2-} of the $[Fe_4S_4]$ cluster (*43*, *44*).

Not only does the scheme for disulfide reduction in FTR (Figure 7) provide a rationalization for the novel redox and spectroscopic properties of FTR and NEM−FTR, but it also suggests a mechanism for biological disulfide reduction by an Fe-S cluster in sequential one-electron steps (Figure 8) that incorporates the thiol−disulfide interchange mechanism established for the NAD(P)H-dependent flavin-containing disulfide oxidoreductases (*11*). By analogy with flavoprotein disulfide reductases, we use the terms electron-transfer or cluster-interacting thiol for Cys84, since it accepts electrons and forms a covalent adduct with the cluster, and interchange thiol for Cys54, since it attacks and forms the heterodisulfide intermediate with one of the cysteines of the substrate disulfide. The mechanism shown in Figure 8 is essentially analogous to that previously proposed (*10*), with the only difference now being that the one-electron-reduced intermediates are viewed as cluster-based radical species, i.e., $S = 1/2$ $[Fe_4S_4]^{3+}$ clusters.

The initial formation of the one-electron-reduced intermediate is central to this mechanism, since it then frees the interchange thiol (Cys54) to attack the thioredoxin (T) disulfide to form the heterodisulfide intermediate [(Cys54)S-S(T)]. The second electron then cleaves the cluster-associated μ_3-S-S(Cys84) disulfide allowing the cluster-interacting cysteine to cleave the heterodisulfide and thereby effect complete reduction of thioredoxin disulfide with restoration of the FTR active-site disulfide. This mechanism has two paramagnetic intermediates, one corresponding to the initially formed one-electron-reduced FTR and the other to the subsequently formed heterodisulfide species, and both are likely to involve similar $S = 1/2$ $[Fe_4S_4]^{3+}$ clusters. In accord with this mechanism, two $S = 1/2$ EPR signals are seen on freezing samples during turnover; one is identical to one-electron-reduced FTR ($g = 2.11, 2.00, 1.98$) and the other is a similar slowly relaxing species with smaller g-value anisotropy ($g = 2.07, 2.01, 2.00$). We propose that this latter species corresponds to the heterodisulfide intermediate. True freeze-quench EPR experiments on the millisecond time scale are planned to characterize fully these intermediates and the reaction kinetics.

REFERENCES

1. Knaff, D. B., and Hirasawa, M. (1991) *Biochim. Biophys. Acta 1056*, 93−125.
2. Buchanan, B. B. (1992) *Photosynth. Res. 33*, 147−162.
3. Buchanan, B. B., Schürmann, P., Decottignies, P., and Lozano, R. M. (1994) *Arch. Biochem. Biophys. 314*, 257−260.
4. Iwadate, H., Yano, K., Kamo, M., Gardet-Salvi, L., Schürmann, P., and Tsugita, A. (1994) *Eur. J. Biochem. 223*, 465−471.
5. Falkenstein, E., Vonschaewen, A., and Scheibe, R. (1994) *Biochim. Biophys. Acta 1185*, 252−254.
6. Droux, M., Jacquot, J.-P., Miginac-Maslow, M., Gadal, P., Huet, J. C., Crawford, N. A., Yee, B. C., and Buchanan, B. B. (1987) *Arch. Biochem. Biophys. 252*, 426−439.
7. Huppe, H. C., de Lamotte-Guéry, F., Jacquot, J.-P., and Buchanan, B. B. (1990) *Planta 180*, 341−351.
8. Chow, L.-P., Iwadate, H., Yano, K., Kamo, M., Tsugita, A., Gardet-Salvi, L., Stritt-Etter, A.-L., and Schürmann, P. (1995) *Eur. J. Biochem. 231*, 149−156.
9. Marc-Martin, S., Spielmann, A., Stutz, E., and Schürmann, P. (1993) *Biochim. Biophys. Acta 1183*, 207−209.
10. Staples, C. R., Ameyibor, E., Fu, W., Gardet-Salvi, L., Stritt-Etter, A.-L., Schürmann, P., Knaff, D. B., and Johnson, M. K. (1996) *Biochemistry 35*, 11425−11434.
11. Williams, C. H., Jr. (1992) in *Chemistry and Biochemistry of Flavoenzymes* (Müller, F., Ed.) Vol. III, pp 121−211, CRC Press, Boca Raton, FL.
12. Salamon, Z., Tollin, G., Hirasawa, M., Gardet-Salvi, L., Stritt-Etter, A.-L., Knaff, D. B., and Schürmann, P. (1995) *Biochim. Biophys. Acta 1230*, 114−118.
13. Schürmann, P., Stritt-Etter, A.-L., and Li, J. S. (1995) *Photosynth. Res. 46*, 309−312.
14. Antanaitis, B. C., and Moss, T. H. (1976) *Biochim. Biophys. Acta 405*, 262−279.
15. Dunham, W. R., Hagen, W. R., Fee, J. A., Sands, R. H., Dunbar, J. B., and Humblet, C. (1991) *Biochim. Biophys. Acta 1079*, 252−262.
16. Meyer, T. E., Przysiecki, C. T., Watkins, J. A., Bhattacharyya, A., Simondsen, R. P., Cusanovich, M. A., and Tollin, G. (1983) *Proc. Natl. Acad. Sci. U.S.A. 80*, 6740−6744.
17. Schürmann, P. (1995) *Methods Enzymol. 252*, 274−283.
18. Gaymard, E., and Schürmann, P. (1995) in *Photosynthesis: From Light to Biosphere* (Mathis, P., Ed.) Vol. 2, pp 761−764, Kluwer Academic Publishers, Dordrecht, The Netherlands.
19. Schürmann, P., and Gardet-Salvi, L. (1993) *Chimia 47*, 245−246.
20. Drozdzewski, P. M., and Johnson, M. K. (1988) *Appl. Spectrosc. 42*, 1575−1577.
21. Werst, M. M., Davoust, C. E., and Hoffman, B. M. (1991) *J. Am. Chem. Soc. 113*, 1533−1538.
22. Hoffman, B. M., DeRose, V. J., Ong, J.-L., and Davoust, C. E. (1994) *J. Magn. Reson. 110*, 52−57.
23. Davoust, C. E., Doan, P. E., and Hoffman, B. M. (1996) *J. Magn. Reson. 119*, 38−44.
24. Mims, W. B. (1965) *Proc. R. Soc. London 283*, 452−457.
25. Abragam, A., and Bleaney, B. (1970) *Electron Paramagnetic Resonance of Transition Metal Ions*, Clarendon Press, Oxford.
26. Hoffman, B. M. (1991) *Acc. Chem. Res. 24*, 164−170.
27. Hoffman, B. M., DeRose, V. J., Doan, P. E., Gurbiel, R. J., Houseman, A. L. P., and Telser, J. (1993) in *EMR of Paramagnetic Molecules* (Berliner, L. J., and Reuben, J., Eds.) pp 151−218, Plenum Press, New York.
28. Houseman, A. L. P., Oh, B.-H., Kennedy, M. C., Fan, C., Werst, M. M., Beinert, H., Markley, J. L., and Hoffman, B. M. (1992) *Biochemistry 31*, 2073−2080.
29. Doan, P. E., Fan, C., and Hoffman, B. M. (1994) *J. Am. Chem. Soc. 116*, 1033−1041.

30. Fan, C., Kennedy, M. C., Beinert, H., and Hoffman, B. M. (1992) *J. Am. Chem. Soc. 114*, 374−375.
31. Werst, M. M., Kennedy, M. C., Beinert, H., and Hoffman, B. M. (1990) *Biochemistry 29*, 10526−10532.
32. Telser, J., Smith, E. T., Adams, M. W. W., Conover, R. C., Johnson, M. K., and Hoffman, B. M. (1995) *J. Am. Chem. Soc. 117*, 5133−5140.
33. Mouesca, J.-M., Rius, G., and Lamotte, B. (1993) *J. Am. Chem. Soc. 115*, 4714−4731.
34. Akasaka, K., Ohnishi, S., Suita, T., and Nitta, I. (1964) *J. Chem. Phys. 40*, 3110−3116.
35. Gemperle, C., and Schweiger, A. (1991) *Chem. Rev. 91*, 1481−1505.
36. Middleton, P., Dickson, D. P. E., Johnson, C. E., and Rush, J. D. (1980) *Eur. J. Biochem. 104*, 289−296.
37. Rius, G., and Lamotte, B. (1989) *J. Am. Chem. Soc. 111*, 2464−2469.
38. Sands, R. H. (1979) in *Multiple Electron Resonance Spectroscopy* (Dorio, M. M., and Freed, J. H., Eds.) pp 331−374, Plenum Press, New York.
39. Anderson, R. E., Anger, G., Peterson, L., Ehrenberg, A., Cammack, R., Hall, D. O., Mullinger, R., and Rao, K. K. (1974) *Biochim. Biophys. Acta 376*, 63−71.
40. Dikanov, S. A., and Astashkin, A. V. (1989) in *Advanced EPR: Applications in Biology and Biochemistry* (Hoff, A. J., Ed.) pp 59−117, Elsevier, Amsterdam.
41. Flanagan, H. L., and Singel, D. J. (1987) *J. Chem. Phys. 89*, 5606−5616.
42. Ciurli, S., Carrié, M., Weigel, J. A., Carney, M. J., Stack, T. D. P., Papaefthymiou, G. C., and Holm, R. H. (1990) *J. Am. Chem. Soc. 112*, 2654−2664.
43. Hu, Z., Jollie, D., Burgess, B. K., Stephens, P. J., and Münck, E. (1994) *Biochemistry 33*, 14475−14485.
44. Stout, C. D. (1988) *J. Biol. Chem. 263*, 9256−9260.

BI9729763